J. Fluid Mech. (1982), *vol.* 116 *pp.* 411–430
Printed in Great Britain

Interferometric study of stable salinity gradients heated from below or cooled from above

By W. T. LEWIS, F. P. INCROPERA AND R. VISKANTA
School of Mechanical Engineering, Purdue University, W. Lafayette, IN 47907

(Received 23 February 1981)

Mixing-layer development is investigated in laboratory experiments of salt-stratified solutions which are cooled from above or heated from below through the imposition of isothermal boundaries. A Mach–Zehnder interferometer is used to infer salt and density distributions within stable regions of the solution and to determine the extent of mixing-layer development. In both heating from below and cooling from above, this development differs significantly from that which has been observed for constant heating from below. Although the formation of a secondary mixed layer is observed, it does not lead to the development of additional mixed layers. Instead, the secondary layer eventually recedes, and the existence of a single mixed layer is restored. This behaviour is due to the isothermal boundary and the effect which it has on decreasing the heat transfer to or from the solution with increasing time. Once the condition of a single mixed layer is restored, extremely large (stable) density gradients develop in the boundary layer separating the mixed and stable regions, and subsequent growth of the mixed layer is slow. In cooling from above, mixing-layer development depends strongly on whether the isothermal boundary is in direct contact with the solution or separated by an air space.

1. Introduction

Buoyancy-driven convection in double-diffusive, thermohaline systems has been studied extensively, and a key feature of the process is the existence of convective (mixing) layers separated by non-convective (diffusive) interfaces. Two different situations have been considered. In one case, the convecting-layer depths and conditions are pre-established, and heat and mass transfer across the diffusive interface(s) are investigated. In the second case, the convecting-layer depth is initially zero, and layer growth is initiated by the double-diffusive process. It is this second situation which is considered in the present study.

Turner & Stommel (1964) and Turner (1968) were the first to consider double-diffusive mixing-layer growth by heating a salt-stratified solution from below. With the initiation of heating, a mixed layer gradually develops from the bottom, and a thermal boundary layer develops above the advancing front of the mixed layer. Boundary-layer development is a consequence of heat diffusion from the mixed layer, and the process of diffusion plays a prominent role within the boundary layer. Temperatures within the mixed and boundary layers increase with time, and the layers continue to grow until the boundary layer becomes unstable. The instability, which occurs in the form of overstable oscillations and may be approximated by linear-

stability theory (Baines & Gill 1969; Turner 1973), results in the formation of a second mixed layer, which is separated from the first layer by a diffusive interface. A thermal boundary layer develops ahead of the second mixed layer, which continues to grow until a third mixed layer is formed. As new mixed layers are formed, it is only the top layer which grows, while the lower layers remain of fixed height. Moreover, as new layers are produced at the top of the system, diffusive interfaces are eliminated at the bottom, as the lowest mixing layer joins with that above it.

From energy and salt-balance considerations, Turner (1968, 1973) predicted the lower-layer growth which results from a uniform bottom heat flux and, by introducing results from linear-stability theory, predicted the maximum height achieved by this layer. Huppert & Linden (1979) retained many features of Turner's work in developing a model for secondary-layer development. Applying energy and salt balances to each of the mixed layers and using the results of linear-stability theory, they predicted the formation of new layers resulting from a uniform bottom heat flux. Ahead of the advancing front, temperatures were predicted to increase gradually owing to diffusion, until the temperature distribution became unstable and a new layer was formed. The height of the uppermost layer increased as the square root of time, while the thickness of each secondary layer remained significantly less than that of the first layer. The density ratio associated with the lowest interface was predicted to decrease steadily to a value of unity, at which point merger of the adjoining layers occurred.

In spite of the significant progress which has been made, there is still much to be learned concerning mixed-layer development in a double-diffusive, thermohaline system. There is, for example, little known about the nature of this development for a linearly stratified salt solution which is cooled from above. Moreover, little is known about mixing-layer development that occurs due to isothermal, rather than constant-heat-flux, boundaries. New insights into mixing-layer development may also be derived from the use of diagnostic tools not yet applied. In particular, the Mach–Zehnder interferometer may be used to obtain a complete and instantaneous record of the density field in stratified regions, without inserting a large number of probes in the test medium. It may also be used as a flow-visualization device to determine the extent of mixing and the position of mixed layers. Accordingly, a primary objective of this study has been to develop an interferometric procedure for simultaneously obtaining density, temperature and salinity distributions in stratified regions. The procedure has been used to study mixing-layer growth in salt-stratified fluid layers heated from below or cooled from above through the imposition of isothermal, impermeable boundaries.

2. Experimental conditions and measurements

A photograph of the test cell used for the study is shown in figure 1. The side walls are constructed of 25·4 mm thick Plexiglas, and pieces of 150 mm square by 15 mm thick high-quality, optical glass are cemented into openings cut from opposite walls perpendicular to the test beam of the interferometer. The bottom surface of the test cell consists of a 2·5 mm thick copper plate which has 5·0 mm diameter copper tubing soldered to its lower side in a serpentine pattern. By circulating warm water from a Lauda Thermostat (NBSD8/25) constant-temperature bath through the tubing, the

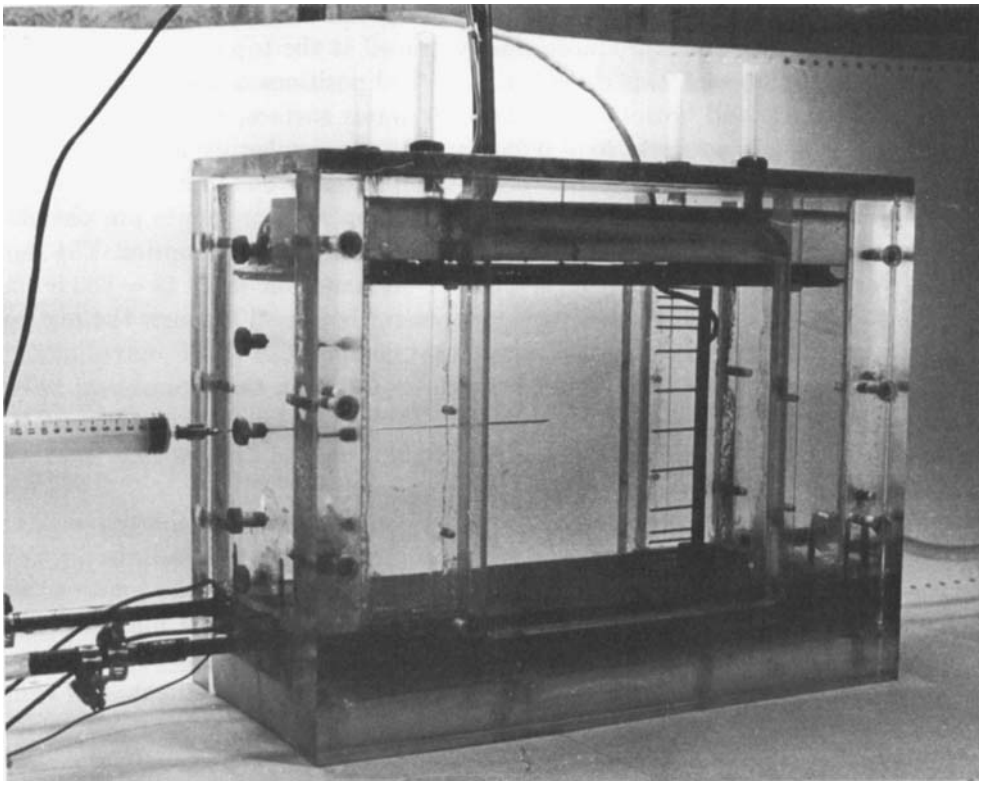

FIGURE 1. Photograph of test cell, including thermocouple probes and sample-extraction probe. Optical-glass windows are at front and back.

bottom surface may be maintained at a uniform temperature which exceeds that of the salt solution. A similar arrangement is used for the top surface of the test cell. In this case, the surface may be maintained at a uniform temperature lower than that of the salt solution by circulating alcohol from a Lauda Ultra Kryomat (TK30D) constant-temperature bath through serpentine tubing soldered to the top of a copper plate. The plate may be maintained in contact with the solution, or it may be separated by an air space. It is sealed to the test-cell sides by a rubber gasket.

The inside dimensions of the test cell provide for a fluid-layer height of $H = 140$ mm, a length (parallel to the interferometer test beam) of $L = 100$ mm, and a width normal to the test beam of $W = 250$ mm. The value of L is restricted by limitations on the fringe density of the interference pattern, while the values of H and W are limited by the size of the interferometer optics. The four side walls are secured with screws, and all joints are sealed with clear silicone glue. Styrofoam (60 mm thick) is used to insulate the side walls, with insulation covering the optical glass being readily removed to allow interference patterns to be photographed. The top and bottom plates are insulated with 30 mm thick Styrofoam.

Holes are drilled in one of the side walls and are provided with fittings which permit the insertion of hypodermic needles. A 3 ml sample of the fluid may thereby be extracted and an analysis performed to determine its salt concentration. A weighing procedure is used for this purpose, and results obtained for standard solutions indicate that the error is less than $\pm 5\,\%$. A thermocouple probe, which is mounted in the test

cell, is used to obtain the vertical temperature distribution. The probe consists of fifteen thermocouples, which are more closely spaced at the top and bottom regions of the test cell. Before each experiment, the vertical positions of the thermocouples, as well as of the top and bottom plates and the water surface, are recorded with a cathetometer which is accurate to $\pm 0{\cdot}05$ mm. Thermocouples are also mounted to the inner surfaces of the top and bottom plates to monitor the boundary temperatures.

Flow visualization and vertical-density-distribution measurements are obtained by using a Mach–Zehnder interferometer with 250 mm diameter optics. The light source is the collimated beam from a 25 mW helium–neon laser ($\lambda = 632{\cdot}8$ nm), which is split into two components. One component is passed through the test cell and is subsequently recombined with the second component, which moves along a reference path. The interference pattern which results from the recombined beams is then photographed. A high-contrast, fine-grain film (Kodak Technical Pan 2415, ESTAR-AH Base) is used to achieve high resolution (15 fringes/mm with the microscope).

The Mach–Zehnder interferometer is used in conjunction with the temperature measurements and a known reference concentration to obtain vertical distributions of the salt concentration and mass density in stratified regions of the solution. The reference concentration is determined by analysing a 3 ml sample of fluid extracted with a hypodermic needle (figure 1). The procedure used to resolve the coupled effects of the temperature and concentration gradients on the density gradient, and hence on the interferometric fringes, is as follows. Each interferogram is analysed using a precision vernier microscope, and the resulting fringe count is read into a data-reduction program, along with the corresponding position and temperature of each thermocouple, the scale factor relating interferometric distances to actual distances, and the position and the concentration associated with the extracted (reference) sample. From knowledge of the fringe shift ϵ associated with a particular position in the solution, the difference between the index of refraction at that position, n, and at the reference position, n_{ref}, is determined from an expression of the form (Hauf & Grigull 1970)

$$n - n_{\mathrm{ref}} = \frac{\epsilon\lambda}{L}. \tag{1}$$

This result is used to obtain the salt concentration at the designated position by comparing it with an alternative expression for the index of refraction. The expression is of the form

$$n = b_0 + b_1 S + S^2, \tag{2}$$

where S is the salt concentration and the constants b_i are obtained from the following procedure. The procedure is based on a curve fit of the form

$$n = a_0 + a_1 T + a_2 T^2, \tag{3}$$

where T is the absolute temperature and the coefficients a_i are known functions of S (Grange, Stevenson & Viskanta 1976). Using the known temperature for the position of interest, the index of refraction is calculated from (3) for a range of salt concentrations associated with the solution. The results are then fitted with a curve to obtain the constants associated with (2). Combining (1) and (2), it then follows that

$$b_0 + b_1 S + S^2 - n_{\mathrm{ref}} = \frac{\epsilon\lambda}{L}. \tag{4}$$

With n_{ref} determined by using (2) with the known value of S at the reference location, (4) is solved for the value of S corresponding to the position of interest. With knowledge of the values of S and T for this position, the mass density ρ is then determined from a curve fit $\rho(S, T)$ of available data (Office of Saline Water 1960). Repeating this procedure for each fringe, the vertical distributions of the salt concentration and mass density are determined for the stratified region of the solution.

The interferograms may also be used to reveal the extent of the mixed regions and the nature of thermal plume penetration into stable regions. For this purpose, the interferometer may be converted to a shadowgraph (by blocking the reference beam) in order to more clearly observe plume penetration. Note that, since the Mach–Zehnder interferometer is a two-dimensional instrument, it provides results which represent averages along the test beam.

Before each experiment, the test cell is cleaned and filled by adding layers of salt solution, with the largest concentration applied to the bottom. The solutions are prepared from distilled water, which is boiled to remove dissolved air, and from analytical grade sodium chloride. From interferograms recorded during the filling process, it was determined that mixing could be minimized, thereby achieving a larger concentration gradient, if filling is achieved with a few thick layers, rather than with many thin layers. Accordingly, three layers are used. At the conclusion of filling, the thermocouple probe is carefully inserted, the test cell is covered with the insulated top plate, and insulated covers are applied to the optical glass windows. The test cell is then left undisturbed for a period of at least two days, during which time all convection currents are eliminated and a uniform temperature and salt-concentration gradient are established. The existence of a linear salt concentration distribution over all but top and bottom fluid layers, approximately 20 mm thick, was confirmed interferometrically.

Just before an experiment, the optical glass covers are removed, and the interferometer is adjusted to an infinite fringe at the very top and bottom of the test cell, where the salt concentration is nearly uniform. Thermal conditions are established in the constant-temperature baths used to heat or cool the fluid, and a sample is extracted with a hypodermic needle, whose location is determined from an interferogram. The positions of the thermocouples, the top and bottom plates, and the fluid layer surface are measured directly with a cathetometer.

The clock is started when circulation through the top or bottom plates is initiated. The plates reach a constant temperature within two minutes and remain within $\pm 0{\cdot}15$ °C of that temperature for the duration of the experiment. Interferograms, temperature scans, and reference concentration samples are taken at prescribed intervals, and the experiment is terminated when mixing-layer growth becomes indiscernible.

Conditions associated with the experiments, whose durations are in the range from $t_f = 80$ min to $t_f = 1950$ min, are summarized in table 1. The initial salt-concentration gradient is in the range $0 \leqslant [m'_{\mathrm{s}} \equiv (\partial m_{\mathrm{s}}/\partial z)_{\mathrm{i}}] \leqslant 0{\cdot}18$ % cm^{-1}, where m_{s} is the per-cent mass fraction of salt in solution and z (cm) is the fluid-layer depth measured from the top surface. The initial temperature difference, ΔT_{i}, is defined as $\Delta T_{\mathrm{c,i}} \equiv T_{\mathrm{i}} - T_{\mathrm{tp}}$ or $\Delta T_{\mathrm{h,i}} \equiv T_{\mathrm{bp}} - T_{\mathrm{i}}$, according to whether the experiment involves cooling from above or heating from below, respectively. The variables T_{i}, T_{tp} and T_{bp} refer to the fluid initial temperature and the top-plate and bottom-plate temperatures, respectively. When cooling from above, the bottom plate is maintained at T_{i}; similarly, when

Experiment	Duration t_f (min)	Initial salt gradient $m'_{s,i}$ (% cm^{-1})	Initial temperature difference ΔT_i (°C)	$Ra_{t,i} \times 10^{-8}$	$Ra_{s,i} \times 10^{-9}$	Air gap δ_a (mm)
1	16	0	$\Delta T_{h,i} = 10$	—	0	3·25
2	16	0	$\Delta T_{c,i} = 10$	—	0	2·90
3	120	0·17	$\Delta T_{c,i} = 10$	5·15	1·84	2·25
4	90	0·17	$\Delta T_{c,i} = 5$	2·29	1·61	2·85
5	100	0·13	$\Delta T_{c,i} = 10$	4·85	1·34	0
6	1200	0·17	$\Delta T_{c,i} = 7$	2·66	1·75	4·03
7	1950	0·15	$\Delta T_{c,i} = 10$	3·79	1·39	0
8	80	0·16	$\Delta T_{h,i} = 5$	3·32	1·74	3·05
9	105	0·125	$\Delta T_{h,i} = 10$	6·75	1·34	2·90
10	120	0·18	$\Delta T_{h,i} = 10$	6·05	2·25	2·95
11	120	0·18	$\Delta T_{h,i} = 5$	2·73	2·44	3·03

TABLE 1. Experimental conditions

heating from below, the top plate is maintained at T_i. Thermal and saline Rayleigh numbers of the form

$$Ra_t \equiv \frac{g\beta_t \Delta T d^3}{\alpha\nu}, \quad Ra_s \equiv \frac{g\beta_s \Delta m_s d^3}{\alpha\nu} \qquad (5), (6)$$

are also tabulated for the initial conditions, where g is the gravitational acceleration, β_t and β_s are the thermal and saline expansion coefficients, α and ν are the thermal diffusivity and kinematic viscosity, respectively, ΔT and Δm_s are the temperature and concentration differences associated with the stable layer, and d is the stable-layer thickness. Since $Ra_{s,i} = 0$ for experiments (1) and (2) (no salt stratification), conditions are expected to be statically unstable. Conversely, since $Ra_{s,i} > Ra_{t,i}$ for the remaining experiments, they are expected to be statically stable. Note that the corresponding density ratios, $R_{\rho,i} \equiv Ra_{s,i}/Ra_{t,i}$, are in the range from approximately 2 to 9. The quantity δ_a refers to the thickness of the air gap separating the top plate and the fluid-layer surface.

In the results which follow, interferograms and temperature, concentration, and density profiles are presented at different times for selected experiments. Symbols on the vertical-temperature distributions originate from each of the specific thermocouple probe measurements. However, although the concentration distributions are obtained from the interferograms, and concentrations are calculated for every fringe which can be resolved, the fringes are too closely spaced to permit use of a symbol for each concentration. Accordingly, a line has been drawn through each of the calculated points, and symbols have been plotted every 30 points to differentiate between results obtained at different times. When viewing the interferograms, several extraneous features should be ignored. These include the thermocouple probes and the hypodermic needle, which are in the fluid, as well as a small turning mirror, which is part of the optical system and external to the fluid. When it appears, the mirror will be seen as a dark rectangle at the end of a supporting rod.

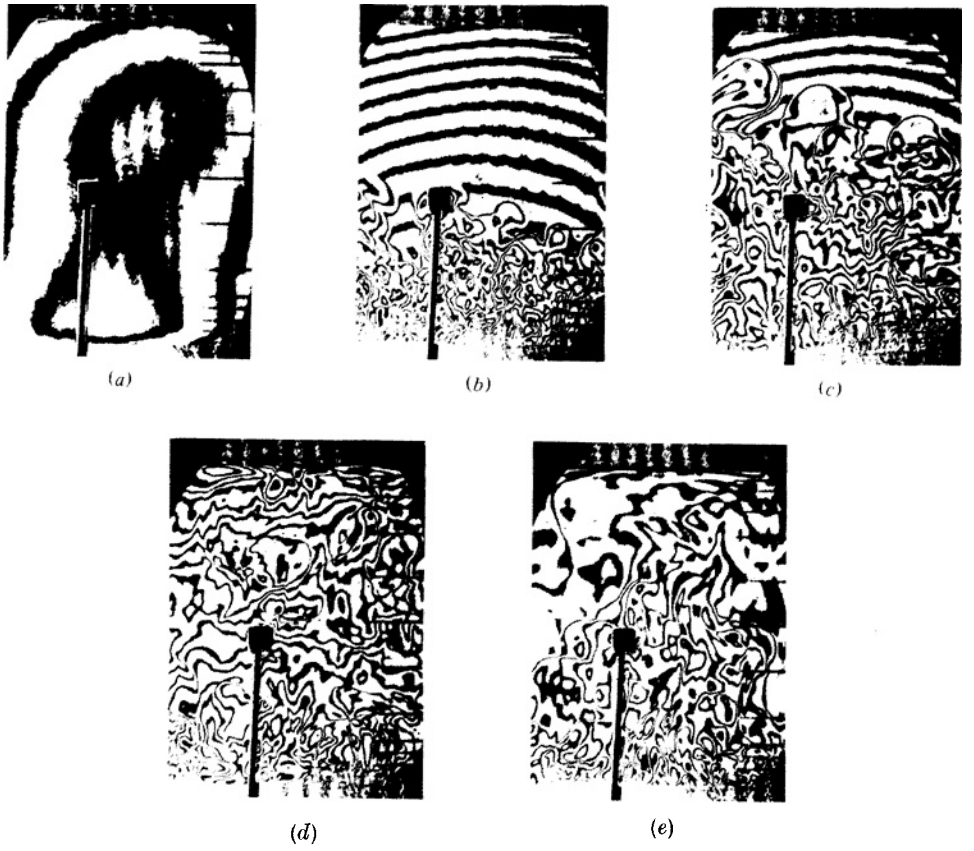

FIGURE 2. Selected interferograms for unstratified water layer heated from below. Experiment (1): (*a*) $t = 0$ s, (*b*) 30 s, (*c*) 45 s, (*d*) 60 s, (*e*) 930 s.

3. Experimental results and discussion

3.1. *Heating from below without salt stratification*

Experiments (1) and (2) of table 1, which involve fluid layers initially of uniform density, provide reference conditions against which subsequent results for the salt-stratified fluid layers may be compared. Selected interferograms obtained for experiment (1) (heating from below) are shown in figure 2. Vigorous mixing is observed to occur shortly after the initiation of heating, and within 60 s the mixed layer, which develops from the bottom, encompasses the entire test cell. The interferograms clearly show the penetration of thermal plumes and the degree to which mixing occurs. The corresponding temperature profiles (figure 3) reveal a nearly uniform distribution in all but a very thin thermal boundary, or conduction, layer at the bottom of the test cell. The boundary layer acts as a conducting region across which there is a large destabilizing temperature gradient and from which the thermal plumes emerge. Its thickness is estimated from the interferograms, and the corresponding temperature difference is approximated as the difference between the bottom-plate temperature and the temperature of the first thermocouple outside the boundary layer. Accordingly, the boundary-layer temperature gradient may be estimated and used with Fourier's

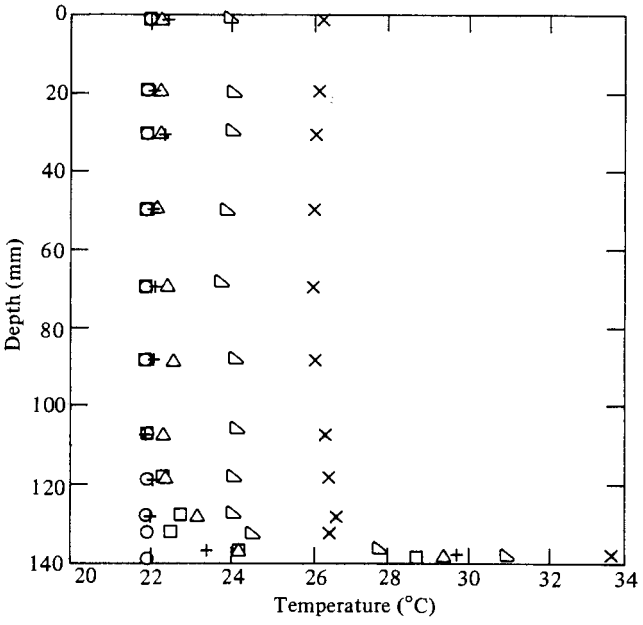

FIGURE 3. Temperature distributions in an unstratified water layer heated from below. Experiment (1): ○, $t = 0$; □, 30 s; △, 45 s; +, 60 s; ◺, 330 s; ×, 930 s. $\Delta T_{b,1} = 10$ °C.

law to predict the bottom heat flux. Values in the range from 4000 to 5000 W m^{-2} are obtained. Owing to this large flux, the uniform temperature associated with the mixed layer increases significantly during the experiment.

Similar trends are associated with experiment (2), although mixing, which develops from above, is much less vigorous and the fluid-temperature change is much less pronounced. These trends may be attributed to the large thermal resistance associated with the airspace separating the top plate from the fluid. The heat flux across this space is due to radiation and conduction and has been estimated to be approximately 100 W m^{-2}. Since this flux is more than an order of magnitude less than that of experiment (1), it follows that destabilizing fluid-temperature gradients should be much smaller and mixing should be less pronounced. Note, however, that, if the top plate is in direct contact with the fluid ($\delta_a = 0$), the heat flux and destabilizing temperature gradient would be much closer to values associated with heating from below. Mixing would then be more vigorous, and there would be a significant reduction in temperature throughout the fluid.

Similar results have been obtained for thermally stratified solutions heated from below or cooled from above (Behnia & Viskanta 1979, 1980).

3.2. *Salt-stratified solutions cooled from above*

With salt stratification, mixed-layer development is significantly inhibited. For conditions corresponding to cooling from above, representative interferograms from experiments (6) and (7) are shown in figures 4 and 5, respectively.

Although the initial salt-concentration gradient and temperature difference vary slightly between the two experiments, the major change is in the surface condition. In one case, experiment (6), the isothermal plate is separated from the liquid by an airspace; in the other case, experiment (7), direct contact is made. At time $t = 0$,

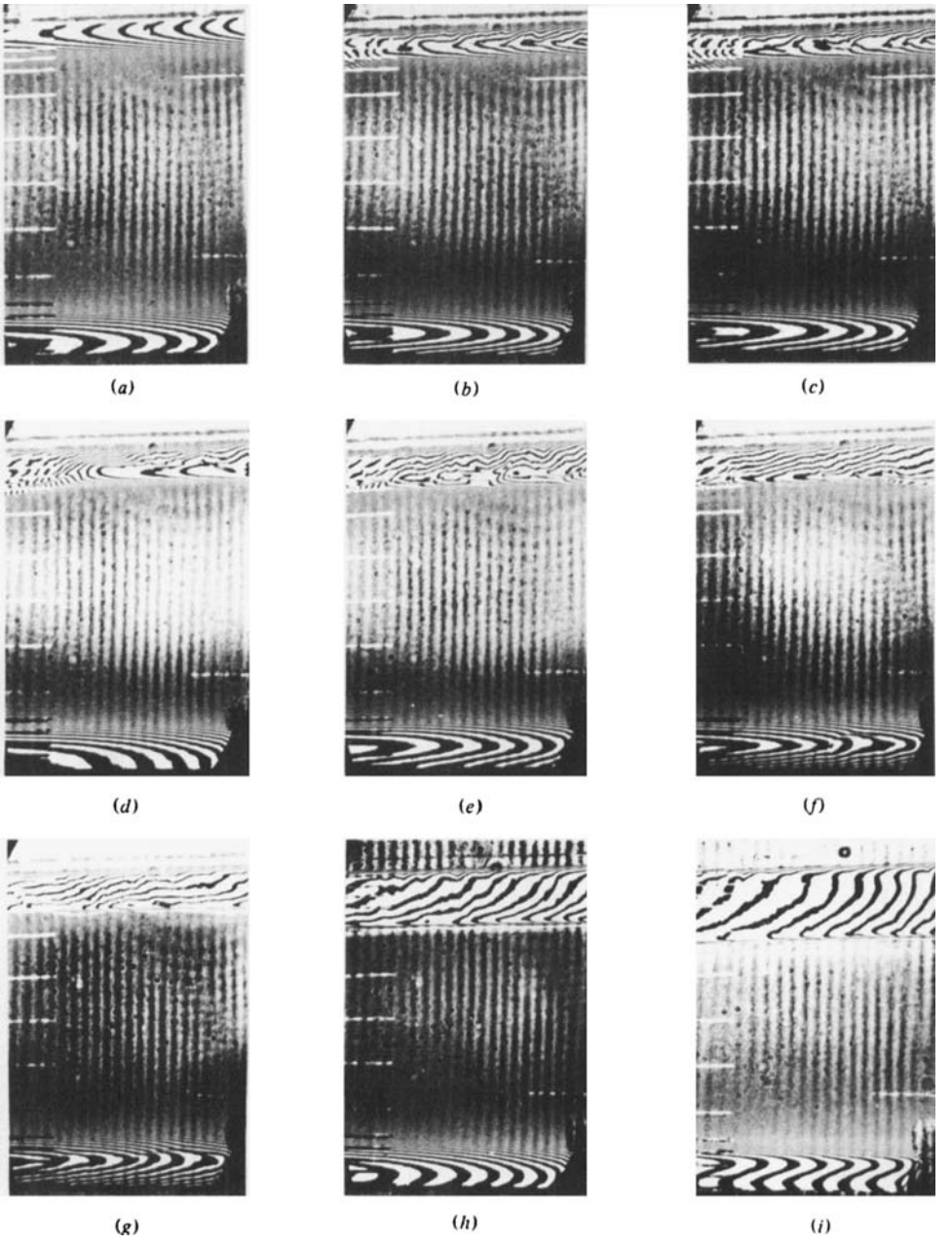

FIGURE 4. Selected interferograms for a salt-stratified water layer cooled from above. Experiment (6): (*a*) $t = 0$ min, (*b*) 4 min, (*c*) 5 min, (*d*) 10 min, (*e*) 20 min, (*f*) 40 min, (*g*) 60 min, (*h*) 300 min, (*i*) 1200 min.

both cases are characterized by a large central layer of positive density gradient, which is bounded by top and bottom fluid layers of nearly uniform density. While the central layer has many horizontal, closely spaced fringes, the top and bottom layers are essentially without fringes. At the start of cooling, both systems are destabilized, and a top mixed layer develops. The layer is characterized by descending,

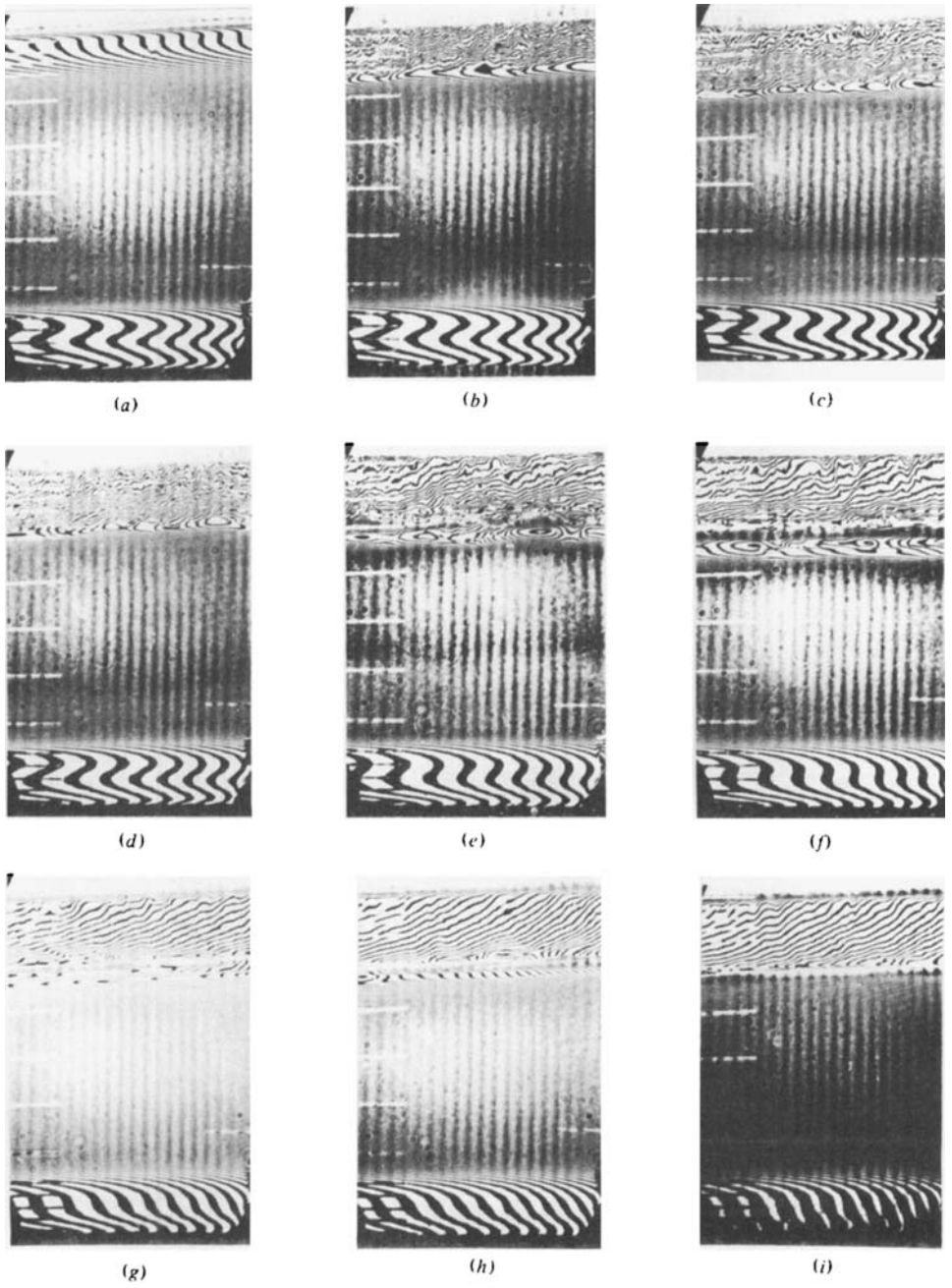

FIGURE 5. Selected interferograms for a salt-stratified water layer cooled from above. Experiment (7): (*a*) $t = 0$ min, (*b*) 2 min, (*c*) 4 min, (*d*) 5 min, (*e*) 10 min, (*f*) 20 min, (*g*) 40 min, (*h*) 60 min, (*i*) 100 min, (*j*) 240 min, (*k*) 360 min, (*l*) 600 min, (*m*) 1200 min, (*n*) 1950 min.

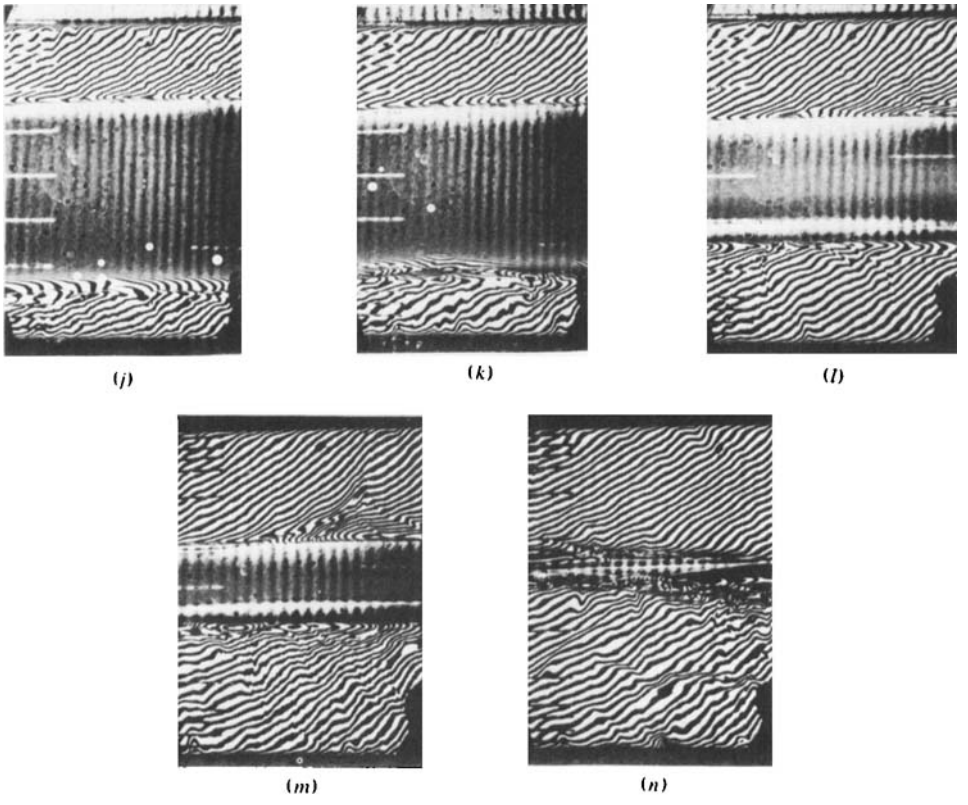

FIGURE 5*j–n*. For legend see p. 420.

mushroom-shaped plumes, which are most evident in figure 5, and it is separated from the stratified fluid by an advancing thermal boundary layer. Contrasting the two experiments, it is evident that, in their early stages, mixing is more vigorous and the mixed-layer growth is more rapid for experiment (7). This difference is due primarily to the effect which the airspace has on the rate of heat removal from the fluid. Using previously described procedures, the initial heat loss is estimated to be approximately an order of magnitude larger for experiment (7) ($H > 2000$ W m^{-2}) than for experiment (6) ($H \simeq 100$ W m^{-2}).

Another difference between the two sets of results concerns the formation of secondary mixed layers below the top (primary) mixed layer. Such a layer begins to form within the first 10 min of experiment (7) and is visible in figures 5(*e–h*). In contrast, no such layers are revealed in figure 4. The effect may again be attributed to differences in the cooling rate. In experiment (6), the heat-withdrawal rate is simply too small to induce destabilizing temperature gradients in the thermal boundary layer which advances ahead of the primary mixed layer. In support of this result, it should be noted that secondary layers were absent in experiments (3) and (4) but did occur in experiment (5).

Returning to the results of figure 5, it is evident that the primary and secondary mixed layers are separated by an interfacial region that is characterized by a stable density gradient. The upper and lower boundaries of the region are somewhat irregular because of buffeting by convective motions in the mixed layers. The secondary mixed

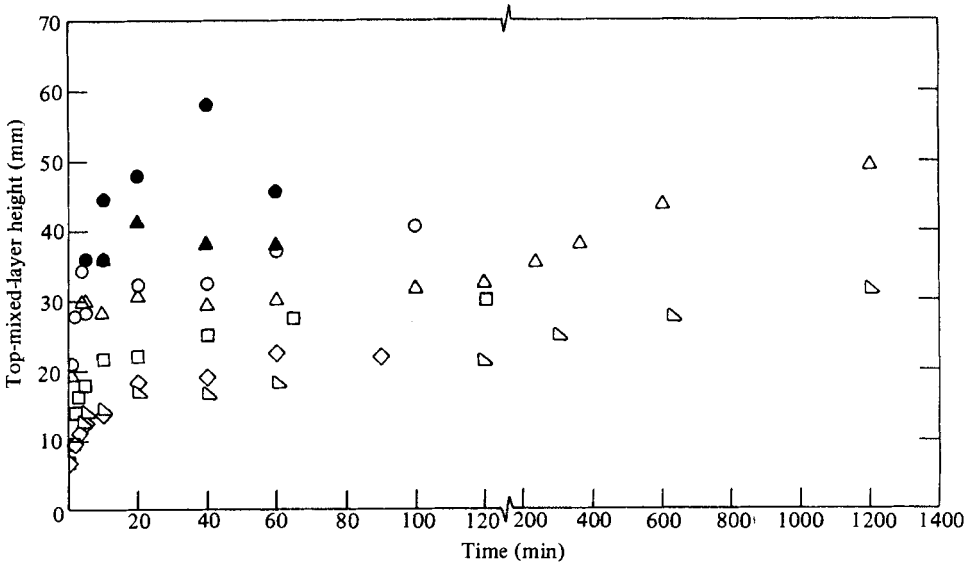

FIGURE 6. Variation with time of primary (open symbols) and secondary (filled symbols) mixed-layer heights for experiments corresponding to cooling a salt-stratified solution from above. □, experiment (3); ◇, (4); ○, ●, (5); ◺, (6); △, ▲, (7).

layer grows until it appears that another mixed layer is about to form (figure 5*g*). This formation never occurs, however, as the secondary layer subsequently recedes until it disappears (figure 5*i*) and there is again a single mixed layer. This behaviour differs from that commonly observed in heating from below, and may be attributed to the different thermal boundary condition. In contrast to the constant bottom heat flux which is typically imposed in experiments involving heating from below (Turner 1968), the surface heat flux in the present experiments decreases with increasing time throughout the experiment. This behaviour results from imposition of an isothermal boundary and the fact that the temperature of the mixed layer approaches that of the top plate with increasing time. In experiment (7), the heat flux at the top surface decreases from a value of approximately 2000 W m^{-2} at 5 min to values of 600, 80 and 25 W m^{-2} at 10, 60 and 1200 min, respectively. This variation has the effect of reducing temperature gradients in the boundary layer ahead of the mixed region, thereby eliminating the development of boundary-layer instabilities.

In the later stages ($t \gtrsim 60$ min) of experiments (6) and (7), conditions are characterized by the slow growth of a single mixed layer. This growth is inhibited by the development of an extremely large density gradient within the advancing boundary layer. The gradient results in very closely spaced fringes which appear as a white narrow band in the interferograms. The band is barely perceptible in figures 4(*g–i*), but is more evident in figures 5(*j–l*). In this region, fringe densities are so large that it is impossible to resolve, and therefore count, the individual fringes. Accordingly, it is not possible to determine the corresponding salt-concentration distributions.

In subsequent stages of experiment 7, which was carried out for an extended period, figures 5(*j–n*) reveal the development and growth of a lower mixed layer. This result suggests that cooling effects have penetrated to the bottom of the test cell, resulting in thermal instabilities and the appearance of ascending thermal plumes.

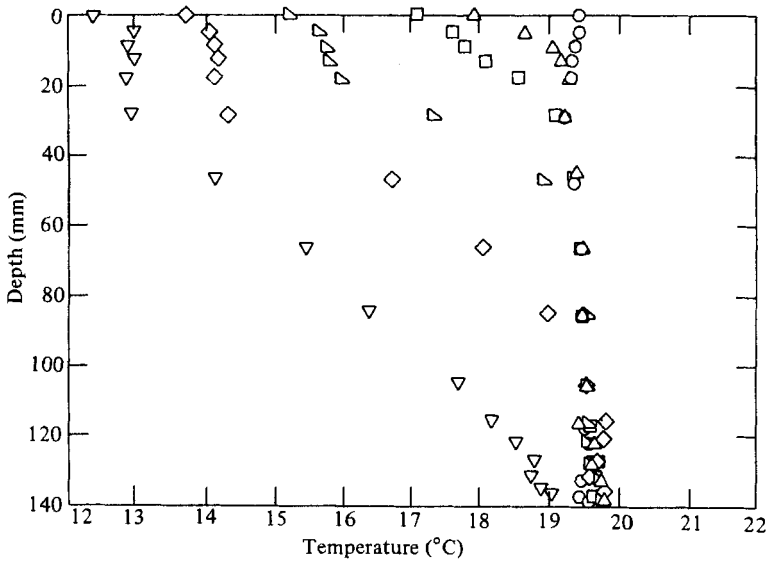

FIGURE 7. Temperature distributions at selected times during cooling from above. Experiment (6): ○, $t = 0$; △, 5 min; □, 10 min; ◺, 60 min; ◇, 300 min; ▽, 1200 min.

Top and bottom mixed layers continue to grow until merger occurs and the entire test cell reaches the temperature of the top plate.

The variation with time of the mixed-layer height is shown in figure 6 for all of the cooling experiments. In each case there is a rapid increase in height during the first ten minutes, after which results depend on whether there is an air space separating the fluid surface from the top plate. Without the air space (experiments (5) and (7)), large cooling rates provide for the development of secondary mixed layers. The height of a secondary layer is represented by filled symbols, while the height of the primary layer is represented by open symbols. The growth and subsequent decay of the secondary layer occurs over a period of approximately 90 min, during which time there is little or no change in the height of the primary mixed layer. Loss of the secondary layer, owing to a reduced cooling rate, is followed by a gradual rise in the height of the primary layer. With the air space (experiments (3), (4) and (6)), small cooling rates preclude the development of secondary mixing layers and, after the first ten minutes, the depth of the primary layer increases gradually with time.

Experiments (6) and (7), which were carried out for extended periods, suggest that, for $t \gtrsim 20$ min, the primary layer grows as t^n. However, the exponent n is less than $\frac{1}{2}$, a value typically ascribed to mixing-layer growth due to constant heating from below (Turner 1968, 1973). The smaller value of n may be attributed to the reduction of the cooling rate with increasing time.

Mixed-layer development is also influenced by the initial temperature difference and salt-concentration gradient, as well as by the air-space thickness. Contrasting the results of experiments (3), (4) and (6) with those of (5) and (7), it is clear that the mixing-layer height increases with decreasing δ_a. Moreover, comparing experiment (5) with (7), it is evident that the layer height increases with decreasing $m'_{s,1}$. Comparing the results of experiment (3) with those of experiments (4) or (6), it also follows that the mixing-layer height increases with increasing ΔT_1. The fact that this result does

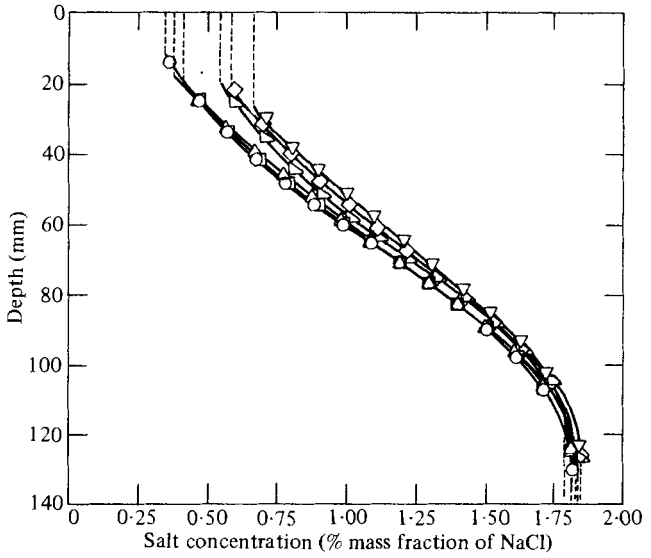

FIGURE 8. Salt-concentration distributions at selected times during cooling from above. Experiment (6): ○, t = 0; △, 5 min; □, 10 min; ◺, 60 min; ◇, 300 min; ▽, 1200 min.

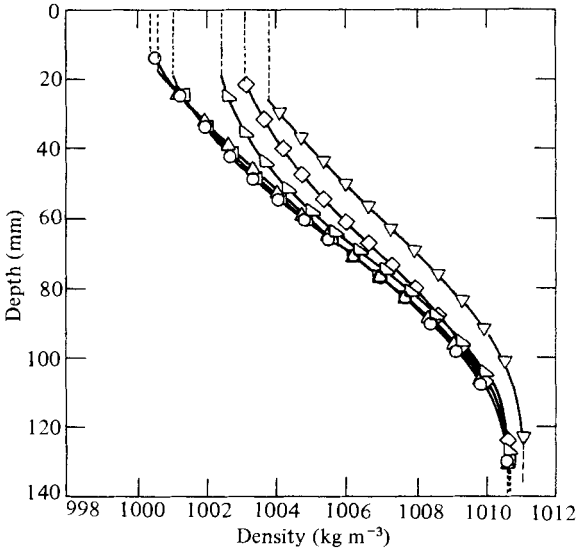

FIGURE 9. Mass-density distributions at selected times during cooling from above. Experiment (6): ○, t = 0; △, 5 min; □, 10 min; ◺, 60 min; ◇, 300 min; ▽, 1200 min.

not follow from a comparison of experiments (4) and (6) may be due to the competing effect of the change in δ_a.

Representative temperature, salt-concentration and density distributions are shown in figures 7, 8 and 9, respectively, for experiment (6). The mixed-layer temperature initially decays rapidly with increasing time, but subsequently decays more gradually as its thermal capacitance increases and the surface heat loss decreases. In addition,

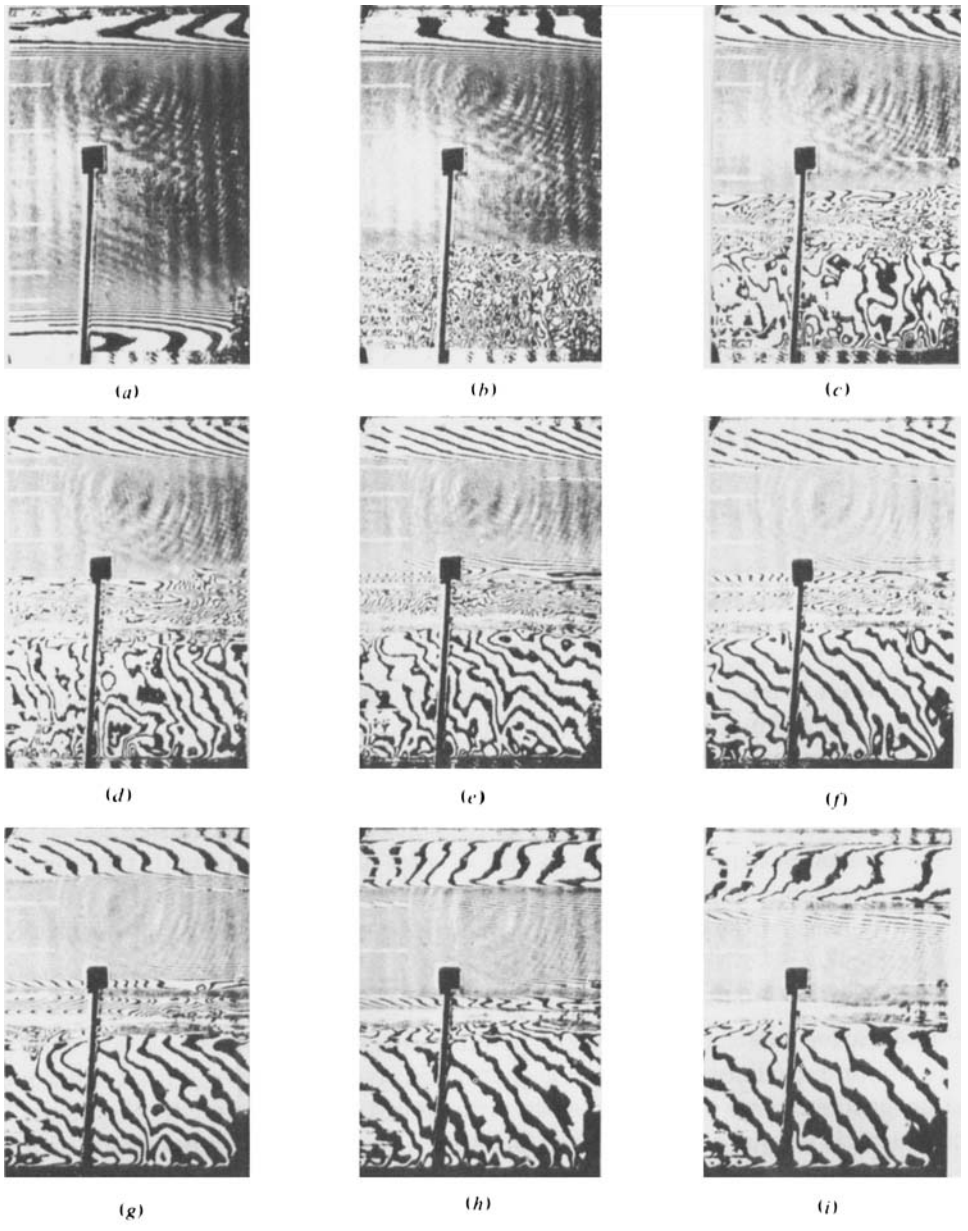

FIGURE 10. Selected interferograms for a salt-stratified water layer heated from below. Experiment (9): (*a*) $t = 0$ min, (*b*) 2 min, (*c*) 5 min, (*d*) 15 min, (*e*) 30 min, (*f*) 45 min, (*g*) 60 min, (*h*) 80 min, (*i*) 105 min.

destabilizing temperature gradients develop below the mixed layer, with stable conditions maintained by the favourable salt concentration gradient. The eventual development of a linear temperature distribution in the stable region is consistent with the imposed surface conditions and is revealed by the $t = 1200$ min results of figure 7. Once cooling effects penetrate to the bottom of the test cell, however, conditions become unstable and a bottom mixed layer begins to develop. This trend is also revealed by the $t = 1200$ min results of figure 7. Cooling is, of course, accelerated if

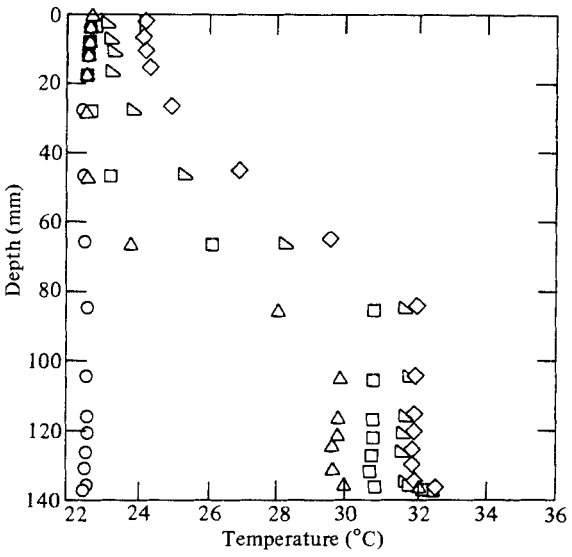

FIGURE 11. Temperature distributions at selected times during heating from below. Experiment (9): ○, $t = 0$; △, 5 min; □, 15 min; ◺, 60 min; ◇, 90 min.

direct contact is made by the top plate, and the bottom mixed layer develops much earlier (at $t = 250$ min for experiment (7)).

As the top mixed layer grows, more highly concentrated salt solution is entrained into the layer, and its concentration increases with time (figure 8). As this growth occurs, however, there is little change in the concentration distribution of the stable region. The mass density of the top mixed layer also increases with time owing to both its increasing salt concentration and its decreasing temperature (figure 9). The gradual increase in the density of the stable region of the fluid is due primarily to the cooling effect.

3.3. *Salt-stratified solutions heated from below*

Representative interferograms corresponding to heating from below are shown in figure 10 for experiment (9), which is characterized by the lowest initial salt-concentration gradient and hence the most pronounced mixing-layer development. The experiment is unique among those of the study, since it is the only one for which R_ρ achieved values of less than 2. From an initial value of $R_{\rho,1} = 1{\cdot}99$, the density ratio decreased with increasing time throughout the experiment, and conditions of monotonic instability were approached. The sequence of events is similar to that associated with cooling from above, except that mixed-layer development is from the bottom rather than the top. Development of the primary mixed layer proceeds rapidly, until a secondary layer begins to form at approximately 5 min (figure 10*c*). Continued growth is confined to this layer up to approximately 20 min, after which it gradually recedes and merges with the primary layer (figure 10*h*). This suspension of growth, which is in contrast to previous results (Turner 1968, 1973; Huppert & Linden 1979), may again be attributed to the reduction in heating which occurs with increasing time. That is, the bottom heat flux is initially large but decreases rapidly as the temperature of the mixed layer increases (figure 11). Estimating the bottom-boundary-layer thickness from the interferograms and approximating the tempera-

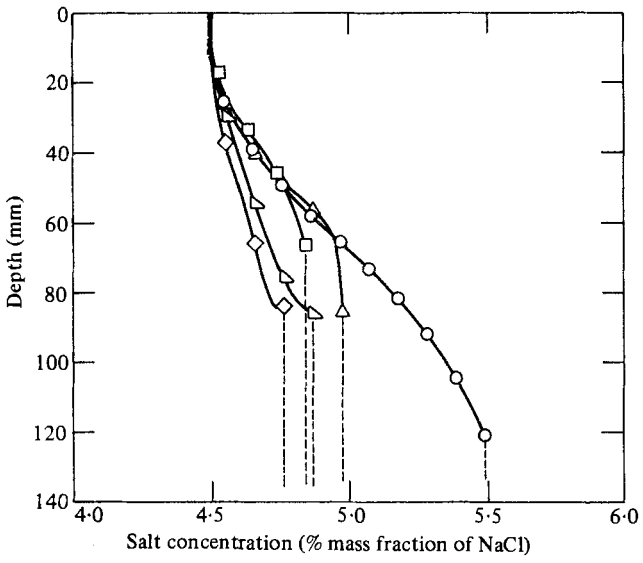

FIGURE 12. Salt-concentration distributions at selected times during heating from below. Experiment (9): ○, $t = 0$; △, 5 min; □, 15 min; ◺, 60 min; ◇, 90 min.

ture difference across the boundary layer as the difference between the bottom-plate temperature and the temperature of the first thermocouple outside the boundary layer, the bottom heat flux is evaluated from Fourier's law. Due to imposition of an isothermal bottom-boundary condition, this flux decreases from a value of approximately 2400 W m^{-2} at 5 min to approximately 200 W m^{-2} at 90 min. In contrast, previous investigators, who imposed a constant bottom heat flux, have observed sustained development and growth of an advancing secondary layer. Although bottom mixed layers would eventually merge, there was no disappearance of the secondary layer, as observed in this study.

Of the four experiments involving heating from below, experiment (9) came closest to achieving complete mixing of the fluid in the test cell. From figure 11, it is evident that, within 60 min, heating effects have penetrated to the top surface and an upper mixed layer has begun to form. Formation and development of this layer is also evident in figures 10(*h*, *i*). Note, however, that, since an air space separates the fluid from the top plate, mixing is not intense and development of the top layer is slow.

The fact that there is a significant change in temperatures ahead of the advancing front of the bottom mixed layer (figure 11) is consistent with values of the flux ratio Q associated with the experiment. With

$$Q = \frac{k\beta_s m_s'}{\beta_t H}, \tag{7}$$

where k and H are the thermal conductivity and bottom heat flux, respectively, values were found to exceed unity throughout the intermediate and latter stages of the experiment. With $Q > 1$, heat transfer from the mixed layer to the stable layer is significant, causing temperature gradients to develop in the stable region.

Although the temperature distribution in the stratified region separating the top and bottom mixed layers has become nearly linear at 90 min (figure 11), stratification

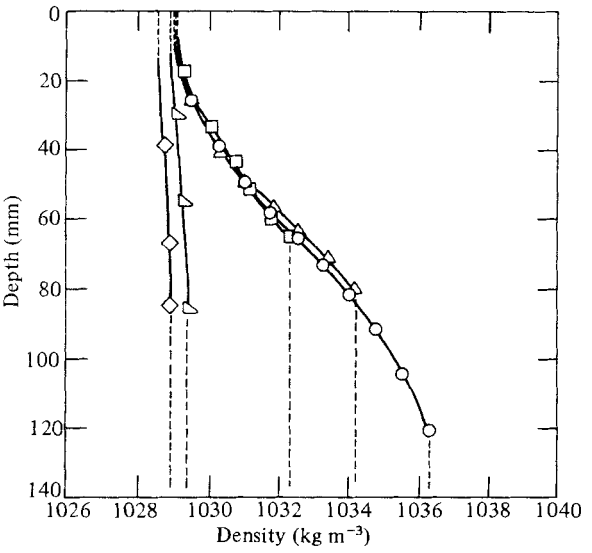

FIGURE 13. Mass-density distributions at selected times during heating from below. Experiment (9): ○, $t = 0$; △, 5 min; □, 15 min; ◺, 60 min; ◇, 90 min.

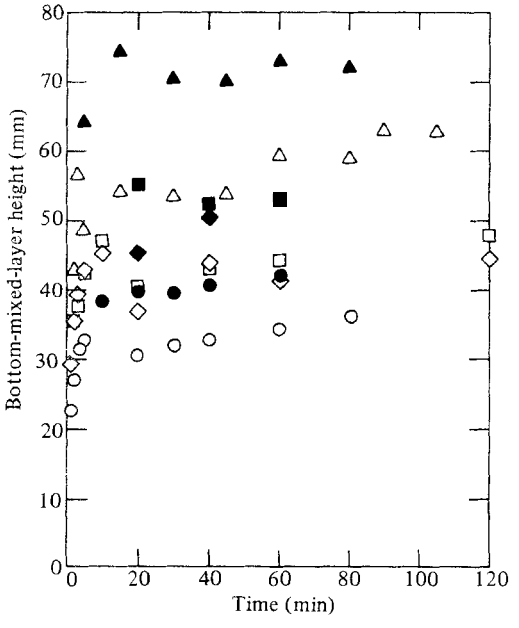

FIGURE 14. Variation with time of primary (open symbols) and secondary (filled symbols) mixed-layer heights for experiments corresponding to heating a salt-stratified solution from below. ○, ●, experiment (8); △, ▲, (9); □, ■, (10); ◇, ◆, (11).

is weak and complete mixing is imminent. The existence of a weakly stratified condition is suggested by the widely spaced fringes associated with figure 10(*i*) and by the concentration and density profiles for $t \geqslant 60$ min in figures 12 and 13, respectively. Despite the negligible stratification indicated by the density profiles of figure 13, however, there exists a large, stable ($d\rho/dz > 0$) density gradient in the boundary

layer that separates the stratified and bottom mixed layers. The fringes in this region, which are too closely spaced to be counted, show up as a white horizontal band in figures 10(*g–i*).

Development of the mixed-layer height is shown in figure 14 for experiments (8)–(11). In each case mixing is vigorous and growth of the bottom mixed layer is rapid for the first 5–10 min, after which a secondary mixed layer appears. The depth h_1 of the primary layer at which the secondary layer begins to form may be compared with predictions based on the assumption of constant bottom heating (Turner 1973)

$$h_1 = \left[\frac{P\,Ra_{t,c}}{64Q}\right]^{\frac{1}{4}}, \tag{8}$$

where P is the Prandtl number and $Ra_{t,c} = 2{\cdot}4 \times 10^4$ is a critical thermal Rayleigh number. For the conditions of experiments (8)–(11), predictions based on equation (8) are in the range 20 mm $\lesssim h_1 \lesssim$ 55 mm for 2000 W m^{-2} $\leqslant H \leqslant$ 5000 W m^{-2}. In view of experimental uncertainties in establishing h_1 and the different bottom-boundary conditions, this range is surprisingly close to that of the experiments.

The depth of the primary layer at which the secondary layer begins to form, as well as subsequent mixed-layer depths, depend upon the imposed initial conditions. Comparing experiments (9) and (10), which correspond to equivalent values of ΔT_i but different values of m'_s, it is evident that mixed-layer development is enhanced by reducing the initial salt-concentration gradient. Similarly, experiments (10) and (11) indicate that development is enhanced by increasing the initial temperature difference. In each experiment the salt concentration and density of the primary mixed layer decrease with increasing time up to the point of merger with the secondary layer. The subsequent increase in these quantities is small and would have been followed by a renewed decay if the experiments had been continued.

Differences associated with cooling from above and heating from below may be inferred by comparing experiments (5) and (9), for which $\Delta T_i = 10$ °C and

$$m'_{s,i} \simeq 0{\cdot}13\ \%\ \text{cm}^{-1}.$$

The most significant difference has to do with the fact that the depth of the primary mixed layer at a time well into the experiment (100 min) is substantially larger (by approximately 20 mm) for experiment (9). Although definite conclusions may not be drawn from a single comparison, it appears that mixing and thermal plume penetration are more significant for heating from below than cooling from above.

4. Conclusions

An interferometric study has been performed of salt-stratified solutions that are heated from below or cooled from above by isothermal boundaries. The major conclusions are as follows.

(i) In both heating from below and cooling from above, mixing-layer development is significantly inhibited by salt stratification. The growth rate and mixing-layer height decrease with increasing initial salt-concentration gradient.

(ii) In cooling from above, conditions depend strongly on whether the liquid is in direct contact with the isothermal heat sink or whether it is separated by an air space. The rate of heat withdrawal for the former condition is initially more than an

order of magnitude larger than for the latter condition. Accordingly, when direct contact is made, mixing is more vigorous, mixing-layer growth is more rapid, and secondary mixed layers will form. Such layers do not appear with the air space, since temperature gradients in the boundary layer ahead of the primary mixed region are too small to provide for destabilization.

(iii) When secondary-layer formation is observed, whether it be for cooling from above or heating from below, the dynamics of its development differ from that which has been reported for constant heating from below. In particular, existence of the secondary layer is temporary. Rather than leading to the development of additional mixed layers, the secondary layer recedes and the existence of a single mixed layer is restored. This result is due to the imposition of an isothermal boundary and the effect which it has on decreasing the rate of heat transfer to or from the fluid, and hence reducing the destabilizing temperature gradients with increasing time. The development and subsequent decay of the secondary layer occurs over approximately 90 min, during which time there is little or no change in the height of the primary layer.

(iv) In the intermediate to later stages of the experiments, following the disappearance of the secondary layers, the boundary layer ahead of the primary mixed layer is characterized by extremely large density gradients, so large that the corresponding interferometric fringes could not be resolved. Such a highly stable boundary layer inhibits growth of the mixed layer, which is substantially less than $t^{\frac{1}{2}}$.

(v) Limited results suggest that mixing-layer development is more pronounced for heating from below than cooling from above.

The work performed in this study was supported by the National Science Foundation under Grant ENG77-22143.

REFERENCES

BAINES, P. G. & GILL, A. E. 1969 On thermohaline convection with linear gradients. *J. Fluid Mech.* **37**, 289–306.

BEHNIA, M. & VISKANTA, R. 1979 Free convection in thermally stratified water cooled from above. *Int. J. Heat Mass Transfer* **22**, 611–623.

BEHNIA, M. & VISKANTA, R. 1980 Dynamics of mixed layer in a nonuniformly stratified fluid heated from below. *A.S.M.E. J. Solar Energy Engng* **102**, 134–141.

GRANGE, B. W., STEVENSON, W. H. & VISKANTA, R. 1976 Refractive index of liquid solutions at low temperatures: an accurate measurement. *Appl. Optics* **15**, 858–859.

HAUF, W. & GRIGULL, U. 1970 Optical methods in heat transfer. In *Advances in Heat Transfer* (ed. J. P. Hartnett & T. F. Irvine), vol. 6, pp. 191–362. Academic.

HUPPERT, H. E. & LINDEN, P. F. 1979 On heating a stable salinity gradient from below. *J. Fluid Mech.* **95**, 431–464.

OFFICE OF SALINE WATER 1960 *Technical Data Book.* U.S. Dept Interior.

TURNER, J. S. 1968 The behaviour of a stable salinity gradient heated from below. *J. Fluid Mech.* **33**, 183–200.

TURNER, J. S. 1973 *Buoyancy Effects in Fluids.* Cambridge University Press.

TURNER, J. S. & STOMMEL, H. 1964 A new case of convection in the presence of combined vertical salinity and temperature gradients. *Proc. Nat. Acad. Sci.* **52**, 49–53.